DYNA-SOAR-GLIDER FLIGHT-ENVELOPE STRUCTURAL PARAMETERS

By Edwin G. Czarnecki and Gordon N. Davison
Boeing Airplane Company

INTRODUCTION

The flight regime of the Dyna-Soar glider is established by both aerodynamic and structural parameters. The upper limit of equilibrium flight on a plot of altitude against velocity is established by maximum lift coefficient, and the lower limits by various structural parameters such as panel flutter, and combinations of loads and temperatures. The structural aspects of the boost phase, orbital flight, and reentry glide are reviewed in this paper.

SYMBOLS

a	panel width parallel to flow, in.
b	panel width perpendicular to flow, in.
C_D	drag coefficient
C_L	lift coefficient
D	hole diameter, in.
E	modulus of elasticity, psi
l	length, in.
L/D	lift-drag ratio
M	Mach number
n_N	structural load factor, normal to vehicle longitudinal axis
q	dynamic pressure, psi

S	planform area, sq ft
t	thickness, in.
W	vehicle weight, lb
α	angle of attack, deg
β	sideslip angle, deg
ϵ	emissivity factor
ϕ	bank angle, deg

Subscripts:

e	effective
MAX	maximum

DISCUSSION

The variation of altitude with time for both a once-around and a twice-around mission is shown in figure 1. The boost phase is characterized by high dynamic pressures, wind shears, and gusts. The orbital phase is associated with low temperatures and micrometeorites. The reentry glide imposes combinations of high temperatures and maneuver loads. These three regions will now be discussed in greater detail.

The flight envelope of the boost phase (fig. 2) may be developed from the known, or expected, normal trajectory of the selected glider-booster combination. The glider recovery ceiling may be defined as the maximum altitude and corresponding velocity from which the vehicle may be recovered if injected into the atmosphere at an entry angle of 0°. It is based on the temperature limits of the various components of the glider, as it operates through the range of lift coefficients from maximum to that at maximum lift-drag ratio. Glide trajectories for both maximum lift-drag ratio at 45° bank angle and maximum lift coefficient are included as reference boundaries for the glider reentry flight regime (shaded area) and will be discussed later with respect to temperatures and loads during the reentry glide. The recovery ceiling is established after the glider is designed for the reentry environment. The boost trajectories should be chosen so that, in the event of boost malfunction, the glider remains below the recovery ceiling.

The wind shear and gust loads occurring in the low-altitude flight regime are critical for the aft fuselage of the glider and are, of course, very important in the design of the booster-glider combination.

The booster and interstage structures have peak temperatures due to aerodynamic heating toward the ends of first- and second-stage boost burnout. The design criteria for these components must account for reasonable deviations from the standard atmosphere and for oscillatory motions of the booster-glider combination.

The panel-flutter placard is of particular interest since it represents a significant item of structural criteria for the glider designer for the boost-phase environment. In the work of reference 1, Hedgepeth showed that $\left(\sqrt{M^2 - 1}\,\frac{E}{q}\right)^{1/3}\frac{t}{l}$ is the governing panel-flutter parameter for isotropic panels. In reference 2, Sylvester presents the results of panel-flutter wind-tunnel tests in terms of this parameter for isotropic panels.

More recently work has been directed toward the skin-corrugation panel-flutter problem. It has been assumed that the same panel-flutter parameter applies with a geometric modification; that is, all geometric quantities are replaced with effective values as indicated in figure 3. These same data are presented by Eldon E. Kordes in a separate discussion of panel flutter, and are shown here for the purpose of completeness in this overall discussion of Dyna-Soar structural parameters.

The temperature history (fig. 4) for a particular point of interest on the lower surface of the glider nose skirt may be represented by a boost-phase peak, moderate cooling during orbit, and a subsequent hot soak during the long reentry glide for the "once-around" mission. The "twice-around" mission exhibits a perigee temperature peak at approximately 90 minutes after launch. This small peak is preceded and followed by moderately low temperature apogee cold soaks. The peak heating is the same for glide reentry from either type of mission, the major difference being the more severe cabin cooling requirements due to greater total heat input in the longer mission.

At altitudes above 250,000 feet, the possibility appears to exist that the glider may sustain slight damage from direct meteoric penetration of its steel surface. According to the latest available information, the daily influx of meteors into the earth's atmosphere is around 11,000 tons. The density of the particles ranges from that of dust to that of iron, but the distribution of density is unknown.

The mass of an individual particle may be estimated by correlation with its visual magnitude (according to M. Dubin of ARDC). The

assumption that all the meteoroids are iron will yield conservative analytical results. For a given mass the diameter of the particle may be determined.

A maximum meteoroid velocity of 250,000 fps and a penetration depth proportional to the particle were assumed, in consultation with the Rand Corporation, and the probability and depth of meteoric penetration were predicted. The relationship between hole diameter D and the probable number of penetrations larger than D per square foot per hour is shown in figure 5. It appears that for a single 0.01-inch-thick skin there will be about 2 penetrations per square foot in 100 hours above 250,000 feet in altitude. Since the glider will spend about 75 minutes above 250,000 feet during a "once-around" mission, and has 330 square feet of planform area, there will be about 8 penetrations greater than 0.0014 inch in diameter per flight. Only one of these will be larger than 0.003 inch and the probability of much larger holes is very small.

Figure 6, the reentry temperature limits for $C_{L,MAX}$, is the first of four figures necessary to portray adequately the relationship of vehicle attitude in equilibrium glide to vehicle component temperature. For high lift coefficients, such as the one shown, there is an area of critical temperature just aft of the transition from nose-cap structure to flat lower surface. An emissivity factor of 0.9 has been used to calculate the 2,700° F temperature limit line for this point "F." There is altitude margin between the limit line and the glide path at the most narrow point around a velocity of 20,000 fps. The more critical of the three heating theories, laminar, turbulent, or transition, is used for design. The laminar theory was critical for this component. The 7.33 limit-load-factor line and the panel-flutter placard are shown as reference limits. The wing loading of 29 psf used in this example is a typical value for a Dyna-Soar glider with medium lift-drag ratio.

The temperature limits shown in figure 7 for an intermediate value of lift coefficient were calculated for the same wing loading as for the maximum-lift-coefficient chart, but involve a different critical glider component. The wing leading edge, swept back 73° and rounded to a 4-inch lower radius, is now the most critical relative to a limiting temperature of 2,700° F. The emissivity factor for this component is also 0.9. The laminar and turbulent limit lines are both shown, and it may be seen that the narrowest altitude margin now occurs at a velocity of around 20,000 fps. An additional design criterion was placed on these limits in that a sideslip angle of 5° was imposed.

The temperature limits shown in figure 8 are for a trajectory at maximum lift-drag ratio with 5° of yaw, and with a 45° bank angle

imposed to provide maximum lateral range. This is actually the critical high-temperature design condition since it has the minimum altitude margin of the three trajectories shown. The cusp usually formed between laminar and turbulent theory temperature limit lines is barely discernible here. The wing loading remains at 29 psf as before, and the leading-edge material is still most critical relative to a limiting temperature of 2,700° F with an emissivity factor of 0.9. The above condition results in a 6,000-foot altitude margin. With a 5° yaw condition and 0° bank angle, the altitude margin is 15,000 feet. With 0° yaw and bank angle, the altitude margin is 21,000 feet.

The variation of glider-component criticality with respect to heating is shown in figure 9. The individual variation of each glider component is represented by the altitude margin between the bank lines shown as references and the lines of altitude plotted against glider angle of attack. The constant velocity of 20,700 fps used in this figure is a typical critical velocity taken from the previous three figures.

The stagnation temperature of the nose cap is invariant with angle of attack, which fact is represented by the horizontal straight line for a 192,500-foot altitude. The heating of the dorsal leading edge of the fin decreases with angle of attack and thus permits a lower operating altitude. The wing leading edge and point "F" exhibit the opposite effect, and thus require higher operating altitudes. The dashed portion of the wing-leading-edge curve is used to account for regions of uncertainty with respect to heating of a highly swept wing leading edge at high angles of attack.

The altitude margin shows the leading-edge structural components to be critical at low angles of attack and the flat plate at point "F" to be critical at high angles of attack.

The glider isotherms shown in figure 10 indicate the maximum upper-surface temperatures encountered during equilibrium glide at 0° bank angle for reentry at maximum lift coefficient and for reentry at maximum lift-drag ratio. The temperatures are based upon an insulated-plate radiation-equilibrium analysis with a surface emissivity factor of 0.9 except as follows: (a) the nose stagnation-point emissivity factor is 0.6 and (b) the leading-edge stagnation-line temperature is reduced 150° F from the insulated case by internal radiation around the leading-edge cell. Aerodynamic heating rates on the upper surfaces are low because of the separated flow conditions, except at the low-lift-coefficient attitude where the windshield cover, the dorsal-fin leading edges, and the forward sides of the fuselage experience high heating rates. Temperatures on the upper aft fuselage have been approximated from flat-plate zero-angle-of-attack conditions and are not affected by internal cross radiation.

The glider isotherms shown in figure 11 indicate the maximum lower-surface temperatures encountered during equilibrium glide for the same flight conditions as in figure 10. The lower-surface isotherms have been determined by using flat-plate equations modified by the three-dimensional delta-wing outflow effects. The outflow effect is responsible for the radical difference in the shape of the isotherms as the vehicle attitude changes from the low- to the high-lift-coefficient case. At low lift coefficient the isotherms are approximately parallel to the wing leading edge and exhibit maximum temperature gradients over the wing surface. At high lift coefficient the isotherms run approximately spanwise and low temperature gradients exist over the entire surface.

All of the lower surface is insulated, as required, to restrict the temperature of the instructure to 2,000° F. The inside face of the lower surface of the wing radiates to the upper wing surface. This is the major factor in determining wing upper-surface temperatures. The temperatures of the lower outer surface directly beneath the fuselage have been computed with no internal cross radiation. The internal cross radiation of an insulated panel does not appreciably affect the outer-surface temperature, but significantly reduces the temperature of the primary structure behind the insulation.

The maneuver capability of the Dyna-Soar glider may be portrayed as in figure 12. The wing loading is 29 psf and the equilibrium glide trajectories for the maximum lift coefficient and maximum lift-drag ratio at 45° bank angle are shown as references. The previous charts explained the criticality of structural heating, relative to vehicle attitude and environment, associated with equilibrium gliding flight at these high and low lift coefficients.

The glider will not sustain steady-state accelerated flight, as experienced in a pull-up maneuver, at altitudes higher than those shown for the various load-factor limits. This maneuver limit exists because the density variation with altitude and the velocity variation do not provide sufficient dynamic pressure. The interesting portion of the curves appears at the cusp points. The cusps are formed where the temperature limit line for the vehicle attitude at maximum lift coefficient, shown previously in figure 6, intersects the constant-load-factor lines established by dynamic-pressure limitations. Therefore, at the cusp of any curve the maneuver capability of the vehicle is limited by temperature at this maximum angle-of-attack condition, but below the cusps, the curves are formed by temperature limits for various points on the vehicle at particular lower lift coefficients along the constant-load-factor lines. Therefore, the structural operational envelope extends between the upper and lower lines in figure 12, but maneuver capability varies with temperature at speeds approaching satellite velocity, dynamic pressure, and elevon system and surface load capacity in the regions of high dynamic pressure.

The load factor referred to in the preceding discussion is computed relative to the vehicle longitudinal axis. The equation used for the determination of this normal limit load factor is as follows:

$$n_N = \frac{C_L qS}{W} \cos \alpha + \frac{C_D qS}{W} \sin \alpha$$

CONCLUDING REMARKS

L 1 1 1 6

A description of the environmental factors which affect the design of the principal components of a Dyna-Soar glider has been given. These factors are panel flutter during the boost phase and reentry at low altitude, and aerodynamic heating and maneuver loads during the hypersonic reentry glide. The components are the skin panels, the nose cap and skirt, and the wing and dorsal-fin leading edges.

Altitude margin was shown to exist between the various equilibrium glide trajectories and the corresponding altitude-velocity relationships for the individual structural components at particular flight attitudes. The variation of these altitude margins with changes in flight attitude, for constant velocity, was also shown. The absolute margins are of course dependent upon the design criteria, such as bank angle, yaw angle, and material limits. The margins also may be changed by local, as well as overall, variations in external and internal configuration. Provision for internal cross radiation is an important aspect of configuration.

The variation of heating along the different glide trajectories was also shown in combination with the changing load-factor capability. A typical glider configuration, such as that designed for a medium lift-drag ratio used in this analysis, has the capability to maneuver to a limit load factor of 7.33 where there is sufficient dynamic pressure available.

[redacted]

REFERENCES

1. Hedgepeth, John M.: Flutter of Rectangular Simply Supported Panels at High Supersonic Speeds. Jour. Aero. Sci., vol. 24, no. 8, Aug. 1957, pp. 563-573, 586.

2. Sylvester, Maurice A.: Experimental Studies of Flutter of Buckled Rectangular Panels at Mach Numbers From 1.2 to 3.0 Including Effects of Pressure Differential and of Panel Width-Length Ratio. NACA RM L55I30, 1955.

[redacted]

DESIGN AREAS

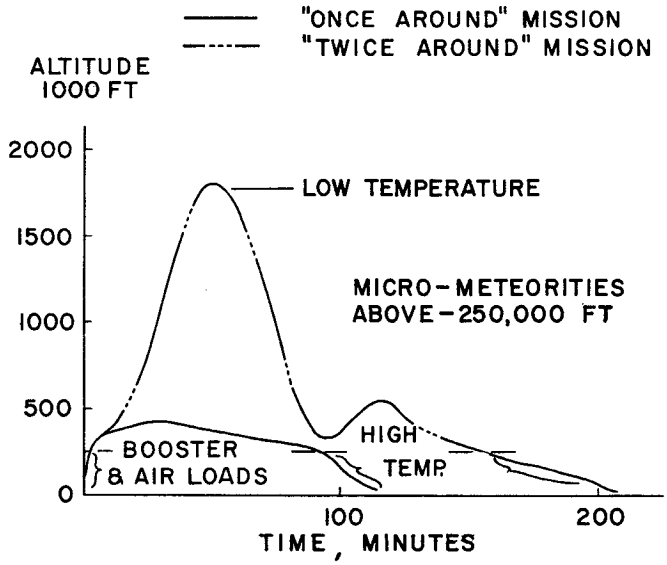

Figure 1

FLIGHT ENVELOPE, BOOST PHASE
W/S = 29 PSF

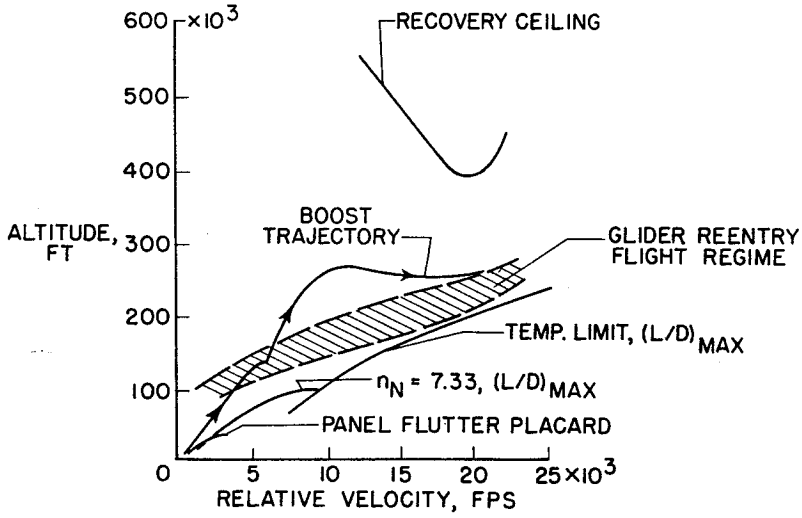

Figure 2

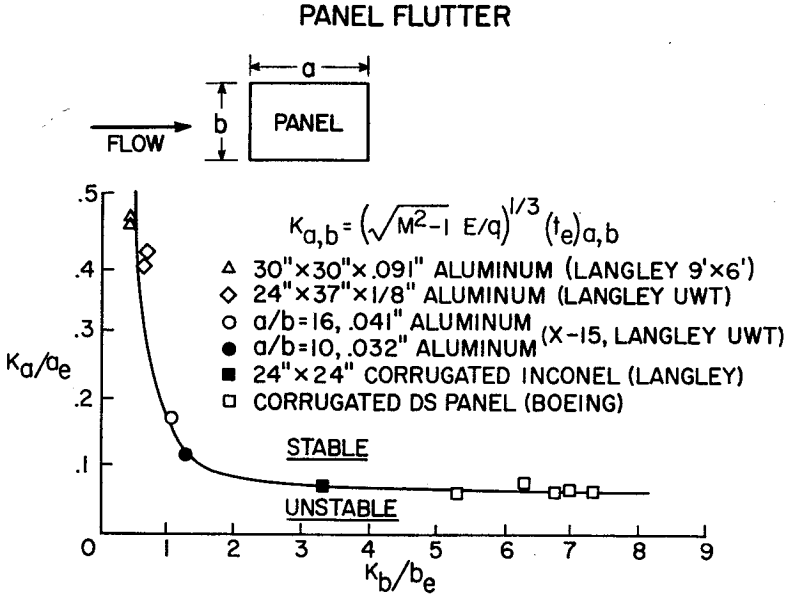

Figure 3

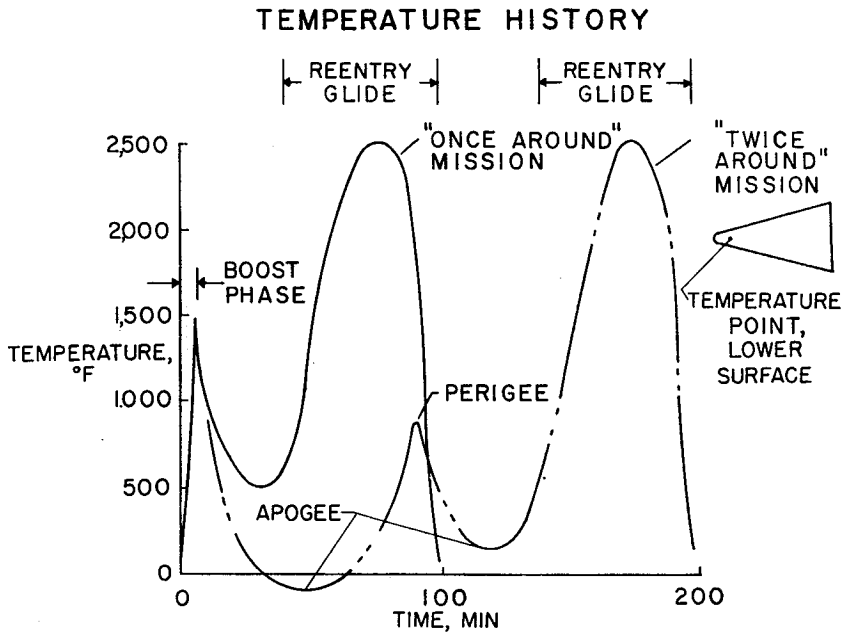

Figure 4

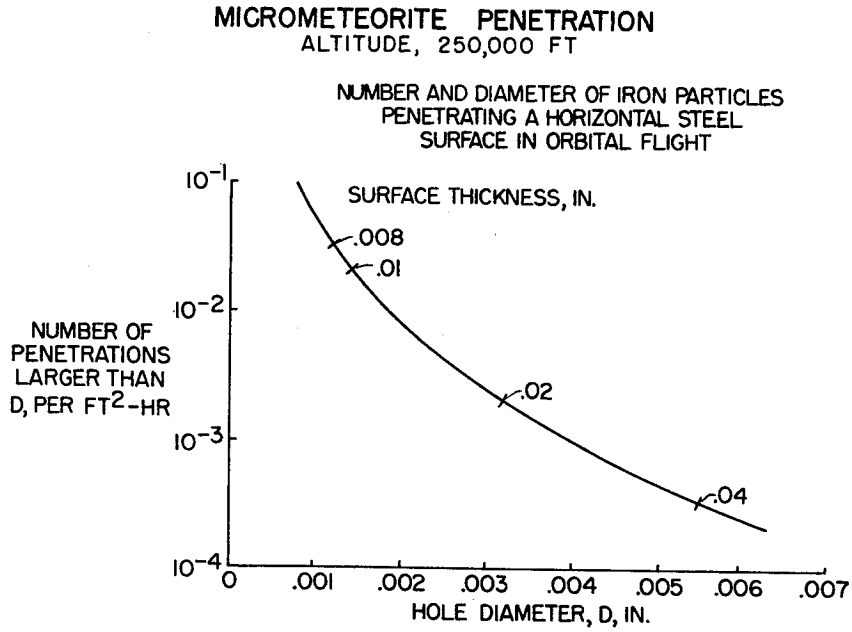

Figure 5

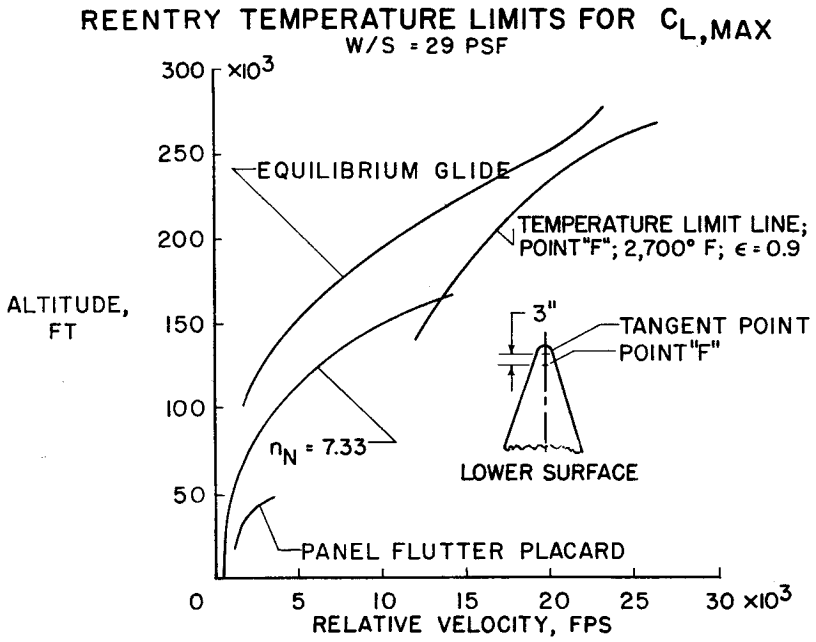

Figure 6

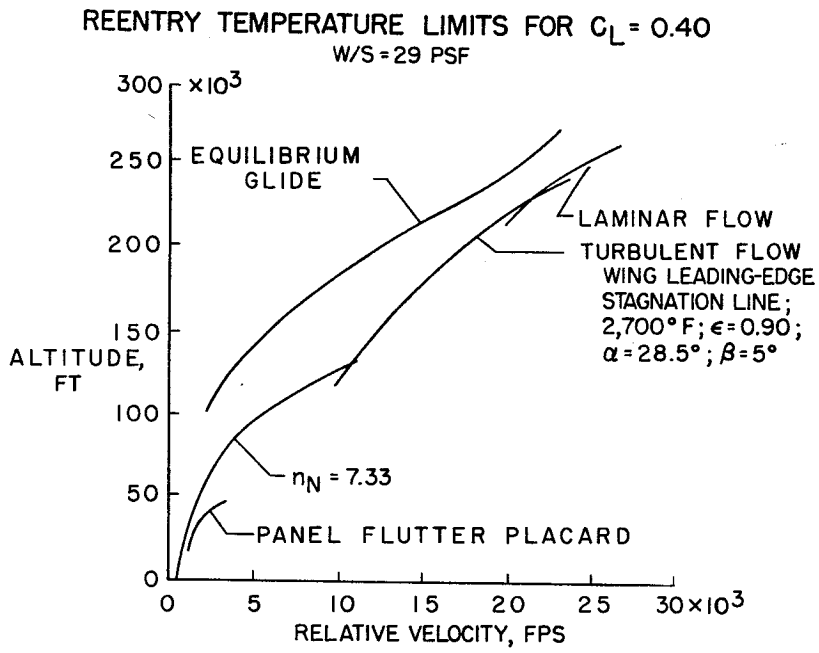

Figure 7

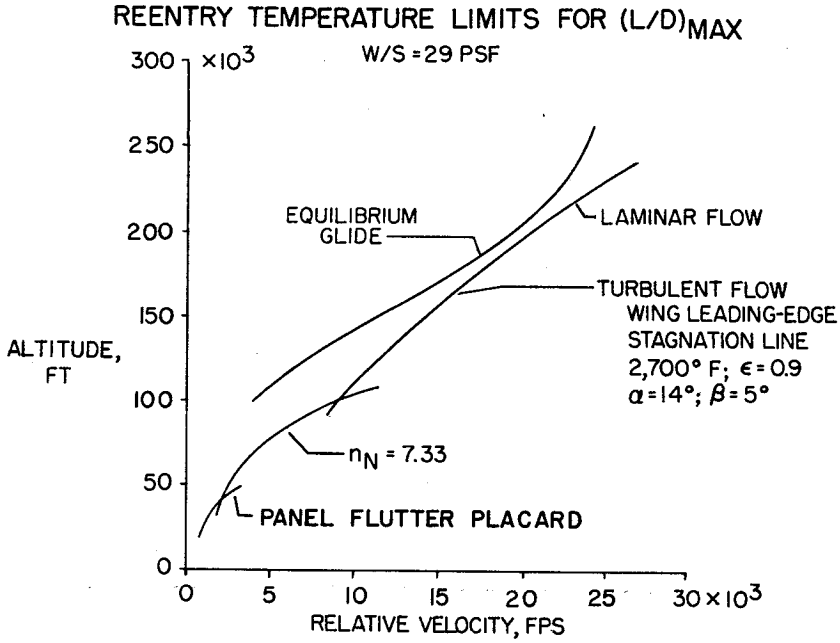

Figure 8

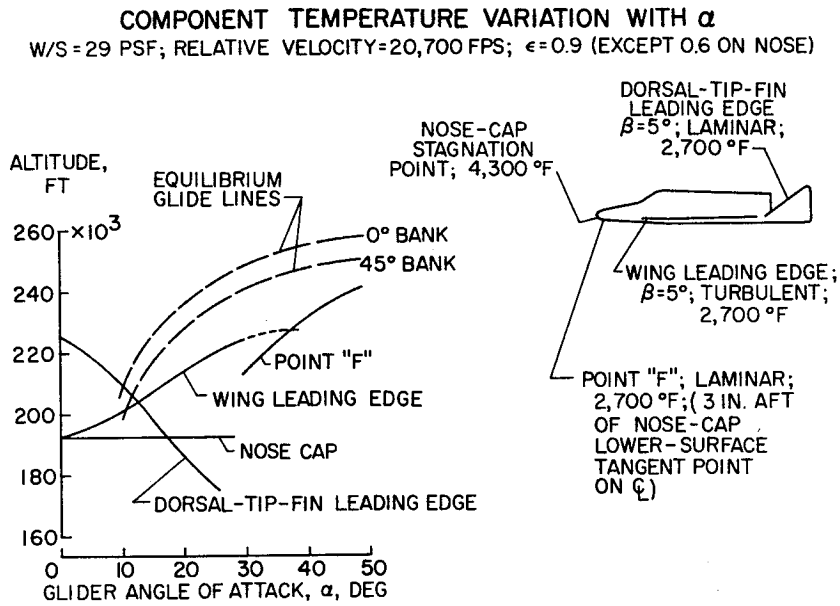

Figure 9

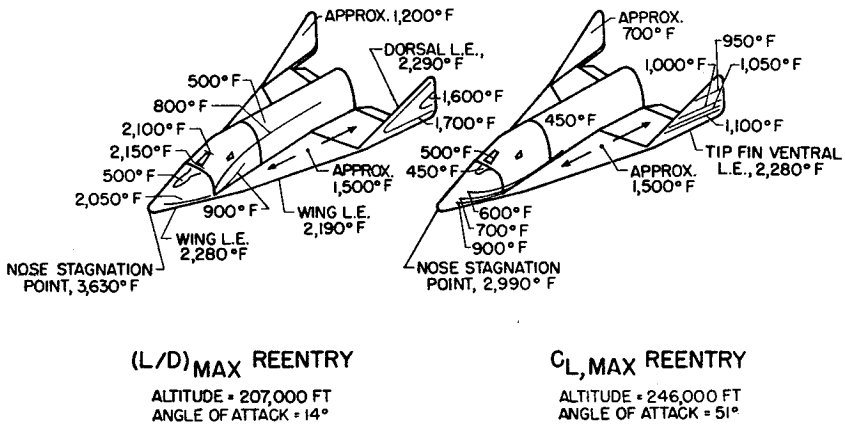

Figure 10

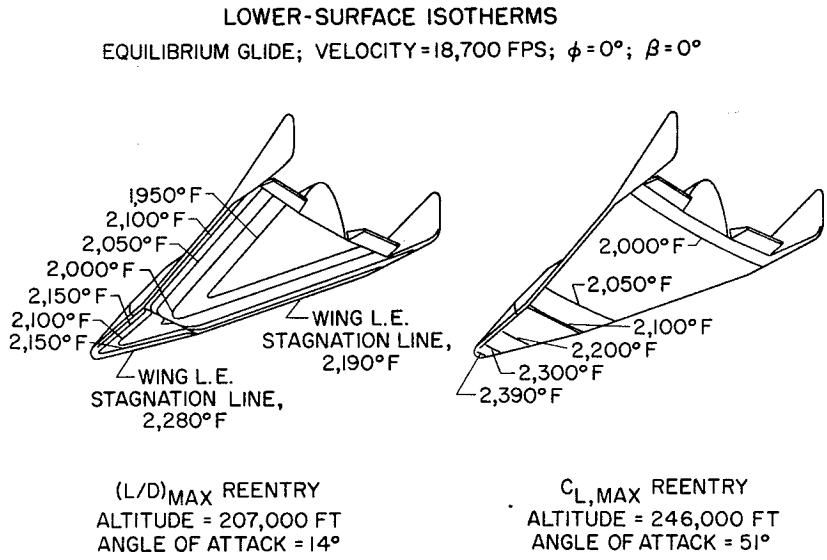

Figure 11

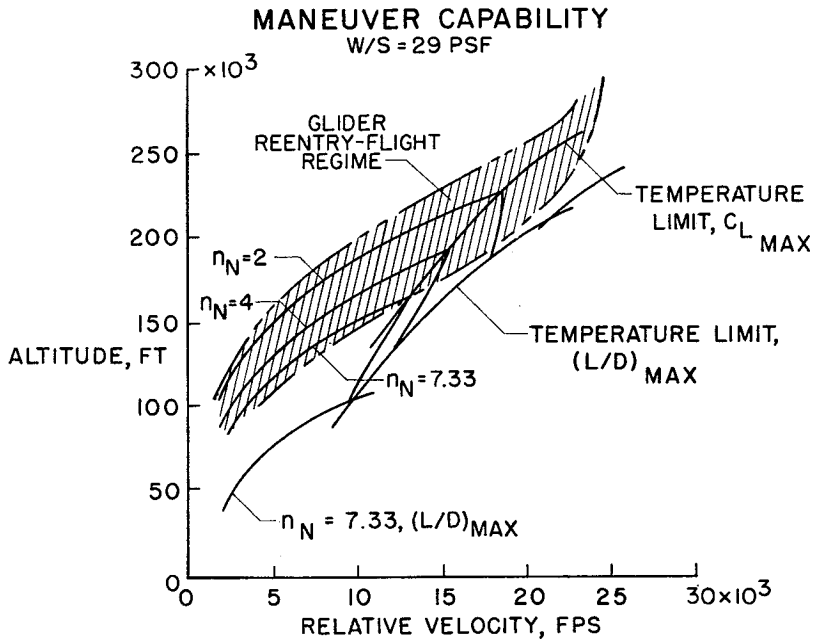

Figure 12